



Experimental investigation of spontaneous imbibition process of nanofluid in ultralow permeable reservoir with nuclear magnetic resonance

Hongda Zhou, Qingsheng Zhang, Caili Dai*, Yuyang Li, Wenjiao Lv, Yining Wu, Rui Cheng, Mingwei Zhao*

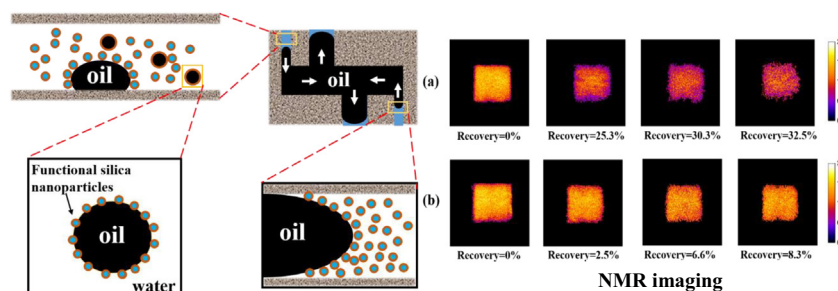
School of Petroleum Engineering, State Key Laboratory of Heavy Oil Processing, China University of Petroleum (East China), Qingdao 266580, PR China

HIGHLIGHTS

- A novel nanofluid based on functional silica nanoparticles was prepared.
- Imbibition and NMR measurement were combined to monitor oil distribution.
- 70.82–71.98 wt% of oil was distributed in mesopores (50 nm < pore size ≤ 3000 nm).
- The NMR spectra and imaging show that the nanoparticles seeped into the core.

GRAPHICAL ABSTRACT

In this work, we employed NMR technique to monitor the migration rule of nanofluid in sandstone cores during the spontaneous imbibition process. And EOR mechanism of the nanofluid was discussed.



ARTICLE INFO

Article history:

Received 3 December 2018
Received in revised form 13 February 2019
Accepted 24 February 2019
Available online 7 March 2019

Keywords:

Spontaneous imbibition
Nuclear magnetic resonance
Nanofluid
Interfacial activity
Enhanced oil recovery

ABSTRACT

Spontaneous imbibition of nanofluid has attracted much interest in enhanced oil recovery (EOR) in ultralow permeable reservoirs. However, the oil distribution in ultralow permeable cores during the spontaneous imbibition using nanofluids has not been discussed in detail. In this study, imbibition experiment and nuclear magnetic resonance (NMR) measurement were used to monitor the migration rule of nanofluid and oil distribution in the imbibition. The results show that 70.82–71.98 wt% of the oil was distributed in mesopores (50 nm < pore size ≤ 3000 nm). The final oil recoveries of cores immersed in different concentrations of nanofluids (0.1 wt%, 0.05 wt%, 0.01 wt%, and 0.005 wt%) and brine were 32.5%, 26.9%, 20.5%, 15.1%, and 8.3%, respectively. The NMR spectra and imaging show that the nanoparticles seeped into the core. Significant insight into the oil distribution during the imbibition of nanofluid is provided.

© 2019 Elsevier Ltd. All rights reserved.

1. Introduction

In recent years, nanofluids have attracted much interest as novel fluids because of their promising applications in different

* Corresponding authors.

E-mail addresses: Daicaili@upc.edu.cn (C. Dai), zhaomingwei@upc.edu.cn (M. Zhao).

enhanced oil recovery (EOR) processes (Zargartalebi et al., 2015; Zhang et al., 2014; Hashemi et al., 2014; Franco et al., 2013; Wong and Leon, 2010; Wei et al., 2016). Compared with conventional fluids such as brine and surfactant solution, nanofluids composed of nanoparticles show special electrical, mechanical, magnetic, and optical properties, exhibiting great potential for EOR (Guo and Aryana, 2016; Li et al., 2017; Sharma et al., 2016; Suleimanov et al., 2011). In previous studies, the EOR potential of

many nanoparticles such as silica (SiO_2) (Hendraningrat et al., 2013; Maas et al., 2010; Perino et al., 2013; Monfared et al., 2016), zirconium oxide (ZrO_2) (Karimi et al., 2012), aluminum oxide (Al_2O_3) (Esfandyari Bayat et al., 2014; Rahmatmand et al., 2016); and titanium oxide (TiO_2) (Nakata and Fujishima, 2012; Ehtesabi et al., 2014) was demonstrated.

Nuclear magnetic resonance (NMR) is a rapid and nondestructive method to evaluate the pore structure and oil distribution of porous media. NMR has been used in gas and oil fields (Lai et al., 2016; Tinni et al., 2015; Meng et al., 2016; Liang et al., 2017). The characteristics of oil distribution in pores can be accurately investigated by combining NMR and spontaneous imbibition. NMR T_2 distribution has also been used to study the factors influencing spontaneous imbibition, such as viscosity ratio, gravity, wettability, and boundary conditions (Zhang et al., 2000; Al-Mahrooqi et al., 2003; Wang et al., 2018).

Previous imbibition studies based on NMR mainly used synthetic brine or reservoir water as the imbibition agent. Yang et al. (2016) studied the water imbibition characteristics of tight cores with different mineralogy, pore connectivity, and pore-size distribution (PSD). They found that well-developed macropores (pore radius > 50 nm) have good pore connectivity and facilitated the majority of oil recovery during water imbibition. Wang et al. (2018) studied the spontaneous and forced imbibition characteristics in tight cores using NMR. In the presence of initial water saturation, the recovery contributions of mesopores ($5.85 \mu\text{m} < \text{pore radius} < 58.5 \mu\text{m}$) dominated in forced imbibition. Hun et al. (2016) investigated the water saturation distribution in shale cores during spontaneous imbibition using NMR. They found that the shale cores imbibed with water have a shorter advancing distance of water saturation front than the tight cores. However, spontaneous imbibition using a nanofluid in ultralow permeable sandstone cores using NMR has been rarely studied.

According to the findings of Hammond and Unsal (2011, 2009, 2010) and Zhang et al. (2014), Wasan and Nikolov (2003), Chengara et al. (2004), Kondiparty et al. (2012), Liu et al. (2012), Kondiparty et al. (2011) et al., mainly capillary force allows a water-based fluid to imbibe into pores and thus push the oil out of pores during spontaneous imbibition in ultralow permeable reservoirs. A nanofluid can displace the oil from a solid surface by low interfacial tension; wettability alteration, and structural disjoining pressure. Hence, it is essential to evaluate spontaneous imbibition using a nanofluid in ultralow permeable sandstone cores using NMR.

In this study, NMR technique was used to monitor the migration trend of a nanofluid in sandstone cores during spontaneous imbibition. A nanofluid based on functional silica nanoparticles with interfacial activity was prepared. NMR tests were carried out to study the characteristics of spontaneous imbibition including porosity, wettability, and oil distribution in cores. Based on the NMR results, PSD, wettability, and movable fluid distribution were evaluated. Spontaneous imbibition experiments indicate that oil recovery was obviously improved by using a nanofluid as the chemical agent for EOR. Finally, the EOR mechanism of nanofluid was elucidated.

2. Materials and methods

2.1. Material and apparatus

The silica sol (10 nm, 30 wt%) used in this study was obtained from Ji Sheng YA. Co., Ltd., China. Adipic acid (AR) was purchased from Aladdin Reagent Co., Ltd., China. Chemicals including *N*, *N*-dimethylformamide (DMF, AR), *n*-heptane (AR), deuterium oxide (D_2O), and sodium chloride (NaCl) were purchased from

Sinopharm Chemical Reagent Co., Ltd. The density of D_2O is 1.105 g/cm^3 . Kerosene with a density of 0.8 g/cm^3 was used as the oil phase. NaCl solution (3 wt%) with a density of 1.123 g/cm^3 was used as the reservoir brine at 25°C . Natural sandstone cores (length 2.5 cm and diameter 2.5 cm) were purchased from Haian Oil Scientific Research Apparatus Co., Ltd. Natural ultralow permeable sandstone cores with a gas permeability of 0.5 mD and a porosity of 14% were used.

The transmission electron microscopy (TEM) images of nanoparticles were obtained using a FEI-Tecna G20 microscope. Fourier transform infrared spectroscopy (FTIR) was carried out using a Nicolet 6700 FTIR spectrometer. Dynamic light scattering (DLS) and Zeta potential measurements were carried out using a NanoBrook Omni laser particle size analyzer purchased from Brookhaven Instruments Co., Ltd. Interfacial tension and interfacial dilatational modulus were measured using a dynamic interfacial oscillatory drop tensiometer (Tracker, Teclis, France). Contact angle measurement was carried out using a contact angle measurement system (Tracker, Teclis, France). The oil distribution in sandstone cores was measured using low-field NMR spectroscopy (MicroMTR12-025v, NIUMAG, China) with a magnetic field strength of $0.28 \pm 0.05 \text{ T}$. The major testing parameters are shown in Table 1. The images of oil distribution in sandstone cores were obtained using a medium-size NMR imaging analyzer (MesoMR23-060H-1, NIUMAG, China) with a magnetic field strength of $0.5 \pm 0.05 \text{ T}$ and resonance frequency of 23 MHz.

2.2. Preparation of nanofluid based on functional silica nanoparticles

Functional silica nanoparticles were synthesized following previous study (Li et al., 2017). Fig. 1 shows the fabrication of functional silica nanoparticles. First, $\sim 10 \text{ mL}$ silica sol and 4 g adipic acid were dispersed in 190 mL DMF. The mixture was stirred at 110°C for 12 h. After cooling to room temperature, the mixture was concentrated in vacuum rotary evaporator. The concentrated mixture was washed with ethanol and centrifugally separated three times. The obtained product was dried in an oven at a temperature of 110°C for 24 h. Finally, functional silica nanoparticles were obtained.

Functional silica nanoparticles (0.1 g) were added to 0.1 L of D_2O . To better disperse functional silica nanoparticles, 1 mol/L NaOH solution was used to adjust the pH of dispersion to 10. A clear dispersion was obtained by ultrasonication at 60°C .

2.3. Spontaneous imbibition tests and NMR measurements

Water and oil are rich in proton (H). NMR experiments mainly monitor the hydrogen nucleus of fluid inside the core pore using the NMR characteristics between a hydrogen nucleus and an intense magnetic field. In this study, D_2O without magnetic moment was used as the aqueous phase, and kerosene with magnetic moment was used as the oil phase. The experimental procedure is as follows:

- (1) Cores were dried at 110°C for 48 h. Then, the weight, gas permeability, and porosity of dried cores were measured (Table 2).

Table 1
NMR parameters.

Parameters		Parameters	
Resonance frequency	12 MHz	Scanning number	200
Echo spacing (TE)	0.2 ms	90° pulse width (P1)	$2.8 \mu\text{s}$
Polarization time (TW)	3000 ms	180° pulse width (P2)	$6.4 \mu\text{s}$
Echo number (NECH)	8000	Signal-to-noise ratio (SNR)	44–45

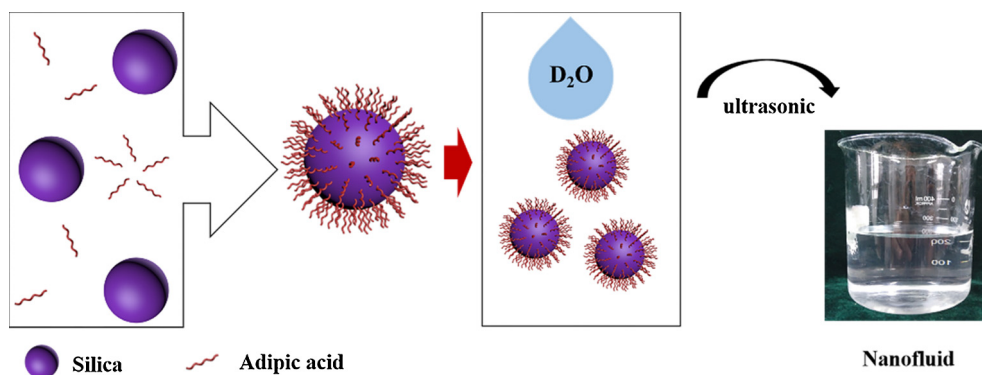


Fig. 1. Schematic illustration of fabrication of functional silica nanoparticles.

- (2) The cores and kerosene were vacuumed for 6 h to remove the gas. Then, the cores were saturated with kerosene under a pressure of 20 MPa for 24 h. The weight of saturated cores was measured (Table 2).
- (3) T_2 distribution and NMR imaging of oil-saturated core samples were measured.
- (4) The cores were immersed in kerosene at 60 °C for 24 h to avoid the effect of kerosene expansion in core pores at experimental temperature. The nanofluid and brine prepared for tests were set at 60 °C for 24 h as well. The above cores were then placed in different fluids in different imbibition cells at 60 °C. The discharged oil was collected into a glass tube with a scale at the top of imbibition cell to record the amount of oil discharged from cores *versus* time.
- (5) The cores were taken out, and the NMR spectra and NMR imaging were measured at selected times during the imbibition. Liquids on the surface of core were dried with cotton yarn, and then the cores were wrapped by a preservative film and Teflon tape (without magnetic moment) to prevent the volatilization of kerosene. Then, T_2 distribution and NMR imaging were measured.
- (6) Step 5 was repeated until the end of experiment, which lasted for 12 days.
- (7) The cores were cleaned with alcohol and benzene and dried in an oven at 120 °C for 24 h. A core slide was chipped out from the dried core and placed in a high-pressure mercury injection (HPMI) apparatus to measure the size of pore and throat.

2.4. NMR theory

The low-field NMR transverse relaxation time (T_2) in porous media is governed by Eq. (1):

$$\frac{1}{T_2} = \frac{1}{T_{2b}} + \frac{1}{T_{2s}} + \frac{1}{T_{2d}} \quad (1)$$

where T_{2b} , T_{2s} , and T_{2d} indicate the bulk relaxation time, surface relaxation time, and diffusion relaxation time, respectively. Compared with surface relaxation, bulk relaxation time is very large

(more than 3000 ms) and generally neglected in sandstone pores. Moreover, in the presence of a uniform magnetic field, diffusion relaxation can also be neglected. Surface relaxation is the main relaxation mechanism for the wetting phase in fluid-saturated rock. The surface relaxation time and pore diameter can be converted using the following equation (Saidian and Prasad, 2015):

$$\frac{1}{T_{2s}} = \rho \frac{S}{V_{\text{eff}}} = \rho \frac{C}{R} \quad (2)$$

$$\rho = \frac{R_p}{T_{2L}C} \quad (3)$$

$$R_p = \frac{2V}{A} \quad (4)$$

where ρ is the surface relaxivity; S is the surface area of rock pore contacted with the fluid; V_{eff} is the effective volume of wetting phase fluid; R is the pore diameter, nm; C is the conversion parameter, the values 1, 2, and 3 are for planar, cylindrical, and spherical models, respectively; T_{2L} is the logarithmic mean calculated by T_2 , ms; R_p is the average pore diameter, nm; V is the total intrusion volume, mL/g; A is the total pore area, m²/g.

Moreover, the distribution of pore sizes follows a fractal scaling and can be described using a fractal model. The fractal models have been described in detail by Zhou and Kang (2016), Zhang and Weller (2014), Zhao et al. (2017) The fractal model is shown in Eq. (5):

$$\log V = (3-D)\log(T_2) + (D-3)\log(T_{2\text{max}}) \quad (5)$$

where V is the accumulative volume fraction of pore throats with relaxation time less than T_2 , $T_{2\text{max}}$ is the maximum value of relaxation time, T_2 is the relaxation time, and D is the calculated fractal dimension ranging from 2.0 to 3.0 (Li, 2010; Cai et al., 2010).

Table 2
Core parameters.

Core parameters	Length (cm)	Diameter (cm)	Permeability (mD)	Porosity (%)	Dried weight (g)	Saturated weight (g)	Kerosene saturability (%)
0.1 wt% nanofluid	2.47	2.52	0.485	14.2	26.18	27.38	95.14
0.05 wt% nanofluid	2.50	2.50	0.535	15.1	28.07	29.37	95.25
0.01 wt% nanofluid	2.48	2.52	0.478	14.7	26.10	27.18	95.96
0.005 wt% nanofluid	2.49	2.50	0.492	15.4	28.67	29.75	96.51
3 wt% NaCl solution	2.48	2.52	0.521	14.9	26.42	27.69	94.77

3. Results and discussion

3.1. Mineralogy

The experiment was based on the Chinese Oil and Gas Industry Standard SY/T5163-2010 (Analysis Method for Clay minerals and Ordinary Nonclay Minerals in Sedimentary Rocks by the X-ray diffraction). The X-ray diffraction (XRD) analysis of sandstone core samples (Fig. 2) shows that the five cores mainly consist of quartz (88.9–91.0 wt%), moderate amount of clay (8.1–10.2 wt%), and slight calcite (1.2–2.0 wt%).

3.2. Characterization of functional silica nanoparticles

The structure and morphology of functional silica nanoparticles were observed using TEM (Fig. 3a). The functional silica nanoparticles exhibited a regular spherical shape with an average diameter of 15 nm, which is conducive to enter the ultralow permeable core. Fig. 3b shows the IR spectroscopy of functional silica nanoparticles. The peaks at 480 and 1100 cm^{-1} were presented due to the bending and stretching vibration absorption of Si—O—Si group, respectively. A peak at 3416 cm^{-1} can be ascribed to the stretching vibration of the OH group. The peaks at 1480 and 2950 cm^{-1} were presented due to the group of —CH₂ and —C—H, respectively. The stretching vibration peak of C=O at 1670 cm^{-1} shows the presence of carboxyl group on silica surface. The FTIR spectra of functional silica nanoparticles indicate that adipic acid was successfully grafted on the surface of silica nanoparticles.

3.3. PSD from NMR

The T_2 relaxation spectrum can effectively reflect the PSD under oil-saturated condition. A longer T_2 relaxation time represents larger pores; in contrast, a shorter T_2 relaxation time represents smaller pores (Meng et al., 2016; Dillinger and Esteban, 2014; Lai et al., 2018). Fig. 4a shows the incremental NMR T_2 porosity spectra of the core immersed in 0.1 wt% silica nanofluid; the cumulative porosity distribution is given as a function of T_2 relaxation time. The T_2 spectrum shows multimodal behaviors, including peak I (0.1 ms < T_2 < 1 ms), peak II (1 ms < T_2 < 100 ms), and peak III (100 ms < T_2 < 1000 ms). The multimodal behaviors are mainly ascribed to the existence of primary intergranular pores, secondary intragranular pores, and minor amounts of micropores (Dillinger and Esteban, 2014; Lai et al., 2016; Wang et al., 2018). Fig. 4a shows that the 100% saturated cumulative porosity is 14.26%, consistent with the result of a routine petrophysical experiment. After imbibition, the cumulative porosity became 6.68%, which can be

regarded as the bound-fluid porosity under spontaneous imbibition condition. The subtraction between 100% saturated cumulative porosity and cumulative porosity after imbibition can be regarded as the movable-fluid porosity, which is mainly attributed to the decrease in peak II.

Eq. (5) shows that the relationship between cumulative porosity distribution and T_2 is linear on a log–log plot. The fractal dimension is a representation of rock heterogeneity and can be used to evaluate the complex degree of pore throat structure, which can be derived from the slope of $\log(V) - \log(T_2)$ plots (Fig. 4b). The curve has a noticeable inflection point at T_2 of 1.0 ms. The slope of plots provides the fractal dimensions for large pores with D_{max} of 2.4617 (3.0–0.5383), consistent with the fractal dimensions of three-dimensional pore spaces ranging from 2.0 to 3.0 (Cai et al., 2010; Giri et al., 2012). However, the slope of line for the small pore is larger than 1.0 (2.1839), which may not follow the fractal model. Generally, fractal dimension is proportional to heterogeneity and complexity (Li and Horne, 2006). The moderate values of fractal dimension (2.4617) indicate moderate complexity and heterogeneity of pore structures.

T_2 can be converted into pore diameter using Eqs. (2)–(4). However, the mercury saturation cannot reach 100% during HPMI measurement. Because NMR T_2 relaxation time reflects the information of tiny pores and throats (Lai et al., 2018), only the right portion of T_2 spectrum ($T_2 > 1$ ms) was selected to determine the surface relaxivity and convert coefficients between T_2 time and pore radius. The calculated surface relaxivity is 29 $\mu\text{m/s}$, whereas the C in Eq. (2) was considered as 2. Fig. 5 shows a good correlation between the calculated PSD from T_2 and HPMI PSD. The conversion relationships between T_2 relaxation time and pore types are shown in Table 3.

The pore system of sandstone can be considered as a dual-scale pore model dominated by movable-fluid pores and immovable-fluid pores. The movable-fluid pores mainly consist of primary and secondary intragranular pores, such as peaks II and III in Fig. 4a. The immovable-fluid pores mainly consist of micropores ($T_2 < 1$ ms) with a complex and heterogeneous pore throat structure, transforming the oil inside to residual oil after imbibition.

3.4. Movable fluid distribution based on NMR

The movable fluid distribution during imbibition can be observed by subtracting the T_2 spectrum after imbibition from that under oil-saturated condition. Fig. 6a shows the T_2 spectrum of core immersed in 0.1 wt% silica nanofluid at different imbibition stages. Under saturated kerosene condition, the maximum peak value of T_2 spectrum is 1150 at 15 ms, indicating that the meso-

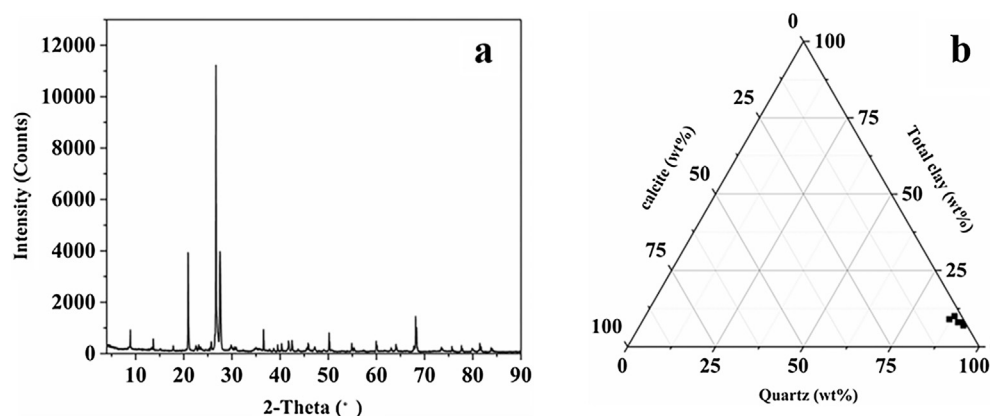


Fig. 2. Mineralogy of five sandstone core samples: (a) XRD spectra, (b) relative contents of minerals.

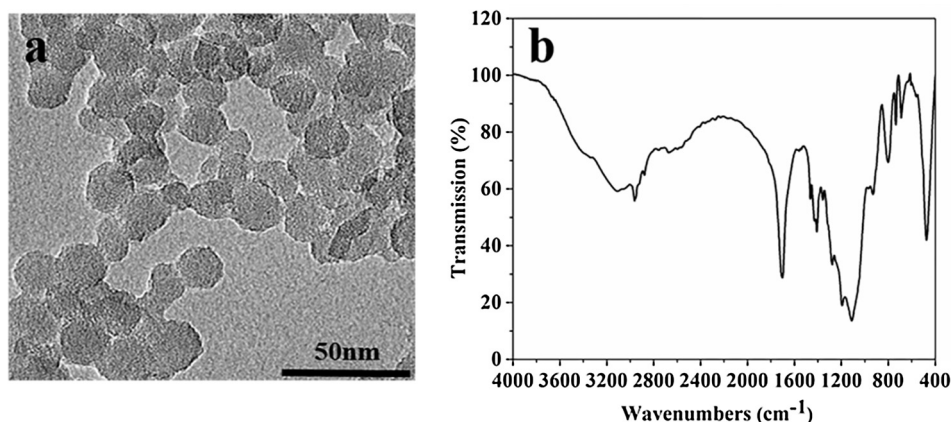


Fig. 3. TEM image (a) and FTIR spectra (b) of functional silica nanoparticles.

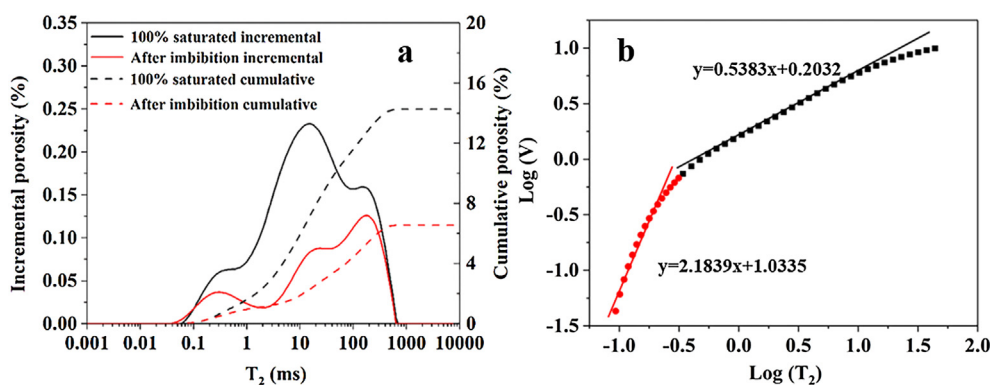


Fig. 4. NMR T_2 incremental and cumulative spectra (a) and relationship (b) between cumulative pore volume V (%) and T_2 (ms).

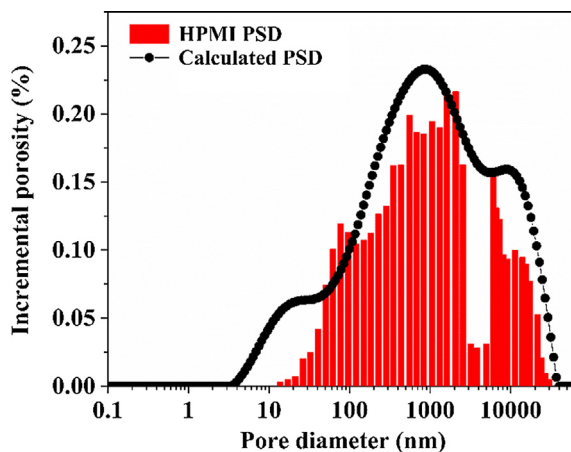


Fig. 5. Comparison between calculated PSD and measured PSD of the core immersed in 0.1 wt% silica nanofluid.

Table 3
Pore classification based on T_2 relaxation time.

T_2 relaxation time, ms	Pore size, nm	Pore type
≤ 1	Pore size ≤ 50	Micropore
$1 < T_2$ relaxation time ≤ 100	$50 < \text{Pore size} \leq 3000$	Mesopore
$100 < T_2$ relaxation time ≤ 1000	Pore size > 3000	Macropore

pores dominate over micropores and macropores. During spontaneous imbibition, the signal amplitude mainly reduced when T_2 relaxation time was between 1 ms and 100 ms. After 12 days, the

signal amplitude barely changed, and the volume of oil in the core no longer reduced. Fig. 6b shows the frequency of oil distribution in pores before and after imbibition. It can be observed that the oil in mesopores is more easily displaced (37.26%) than that in micropores and macropores (3.48% and 1.93%, respectively). The T_2 spectra of remaining samples immersed in nanofluids at different concentrations are shown in Figs. 1S, 2S, and 3S.

In contrast, the T_2 spectrum of core immersed in brine at different imbibition stages shows that the effect of brine on spontaneous imbibition is small (Fig. 6c). After spontaneous imbibition, the signal amplitude of T_2 spectrum decreased, indicating that the oil in the pores was not displaced by immersing in brine. After 12 days, the signal amplitude barely changed, indicating that the volume of oil in the core no longer reduced. As shown in Fig. 6d, the amounts of oil during imbibition displaced by brine in micropores, mesopores, and macropores are only 0.12%, 4.32%, and 0.13%, respectively.

Compared with brine, the signal amplitude of core immersed in 0.1 wt% silica nanofluid clearly decreased after imbibition. This phenomenon can be ascribed to excellent properties of nanofluid. In spontaneous imbibition, capillary force is the main driving force for displacement and increases with the decrease in pore diameter. Under the action of capillary force, nanofluid is continuously imbibed in the deep part of core, and the pore system of core has an instantaneous closed state when the nanofluid is imbibed from all the sides simultaneously. The oil in pores tends to flow out of the core because of increased energy inside the pore system. As the nanofluid seeps into the pores further from the throat, the imbibition energy decreases as the interface increases, and the oil overflows from the core. The flow process was described as a countercurrent flow controlled by capillary forces in the previous

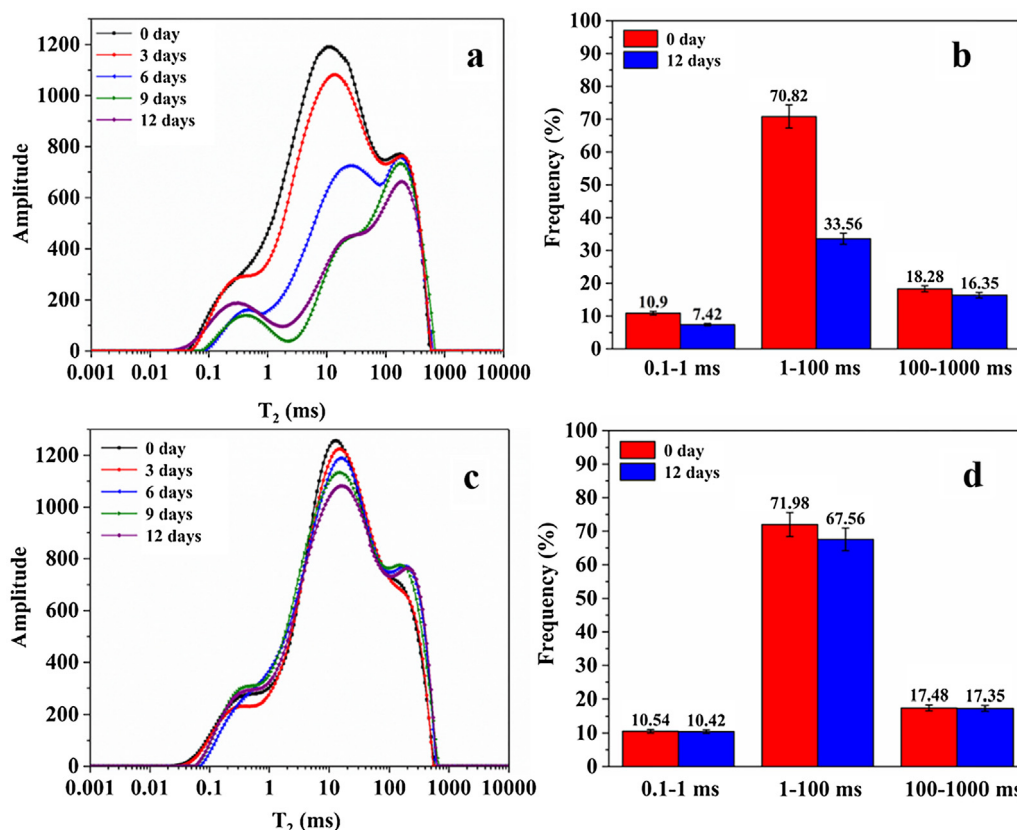


Fig. 6. T_2 spectra during the imbibition of core immersed in 0.1 wt% silica nanofluid (a) and frequency of oil distribution in pores before and after imbibition (b). T_2 spectrum during the imbibition of core immersed in 3 wt% NaCl solution (c) and frequency of oil distribution in pores before and after imbibition (d).

study (Bourbiaux and Kalaydjian, 1990). Owing to the heterogeneity and connectivity of pores, nanofluid is imbibed through small pores, and oil is expelled through large pores simultaneously (Fig. 7a). When nanofluid continues to be imbibed and cuts off the discharge channel, the oil is trapped, and the remaining oil is formed. The nanofluid is first imbibed into micropores and mesopores under the action of capillary force. Then, the oil stored in small pores is expelled from the core through macropores. The oil is filled in pores before imbibition (Fig. 7a). After imbibition, the remaining oil can be divided into two types: oil droplets adhering to the rock wall and oil droplets with nanoparticles adsorbed to the surface. In the later period of imbibition, nanofluid completely enters the pores, and the capillary force is not active for oil expulsion, making it difficult to displace the oil in macropores and forming the remaining oil. Moreover, the oil distribution in micropores before and after imbibition decreased by only 3.48%, indicating

that the oil in micropores was hardly swept by nanofluid and the residual oil was formed after imbibition (Fig. 7b).

Fig. 8 shows the results of spontaneous imbibition tests using different concentrations of nanofluid and brine. The oil recovery using nanofluid increased with increasing concentration. In the initial stage for ~50 h, the oil recovery of core immersed in nanofluid (0.1 wt% and 0.05 wt%) had a rapid increase. After 12 days, the oil recovery of core immersed in different concentrations of nanofluids and brine were 32.5%, 26.9%, 20.5%, 15.1%, and 8.3%. Combined with the results of T_2 spectrum, the recovery contributions of pores mainly focused on mesopores. The result indicate that the silica nanofluid significantly improves the oil recovery of ultralow permeable cores and has a great application potential for EOR.

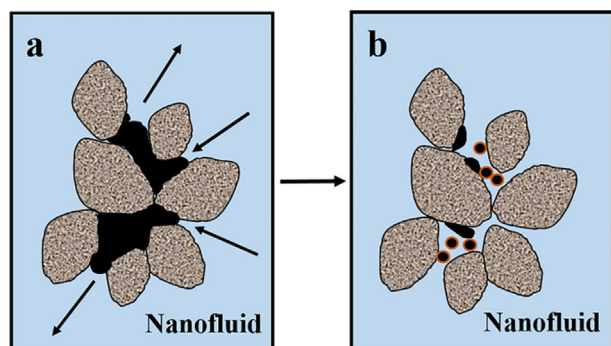


Fig. 7. Schematic diagram of oil distribution before (a) and after (b) imbibition.

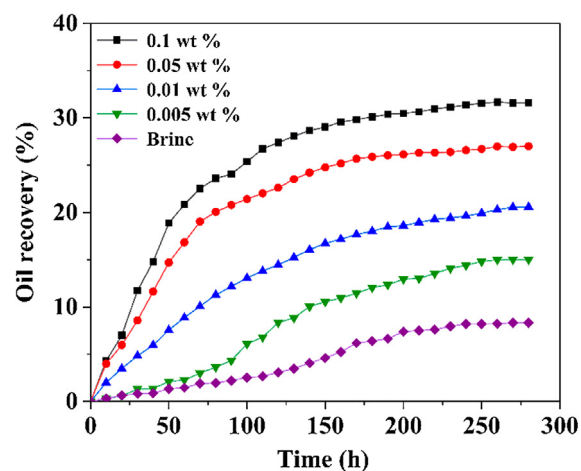


Fig. 8. Oil recovery with time in spontaneous imbibition tests.

3.5. Magnetic resonance imaging (MRI)

To further visualize the oil distribution in core during imbibition, 2D NMR images of core were obtained by NMR imaging (Fig. 9). The total amount of fluid in the core directly affects the strength of NMR signal. The pseudo color image shows the change in kerosene content in core pore (Fig. 9a). Under 100% saturated kerosene condition, the entire core showed a clear yellow color, indicating that the NMR signal was the strongest and the core pore was filled with kerosene. When spontaneous imbibition increased, the intensity of yellow color decreased and became yellow, red, and blue from the middle to the edge. The edge of core appeared to be blurred, and the area became smaller, indicating that the amount of kerosene present at the edge of core decreased first, and then that in the central core decreased. This phenomenon indicates that the kerosene was transported in the core pore with the help of nanofluid. Moreover, the decrease in signal strength was uniform. The front edge of imbibition was relatively uniform, and no obvious advantage channel was formed, clearly indicating the result of spontaneous imbibition.

Fig. 9b shows the 2D NMR images of core immersed in 3 wt% NaCl solution at different imbibition stages. With the increase in spontaneous imbibition time, the distribution of kerosene in the

core and NMR signal barely changed, and the NMR signal intensity was still strong in the middle of core. However, the edge of core appeared to be blurred. This phenomenon indicates that the kerosene was not transported in the core pore, and brine was not very useful for displacing oil from the solid surface. Compared with brine, the silica nanofluid showed good performance in reducing interfacial tension, wettability alteration, and oil displacement.

3.6. EOR mechanism of nanofluid

3.6.1. Interfacial activity of nanofluid

To enhance oil recovery, it is critical to reduce oil–water interfacial tension. The oil–water interfacial tension was 27.8 mN/m at 60 °C. The interfacial tension decreased with increasing nanofluid concentration (Fig. 10a). The interfacial dilatational modulus increased with increasing nanofluid concentration (Fig. 10b). Compared with brine, 0.1 wt% silica nanofluid reduced the interfacial tension to 12.2 mN/m and improved the modulus to 18.5 mN/m. The modulus for interface between nanofluid and kerosene clearly increased, indicating that the adsorption of functional silica nanoparticles at oil–water interface increased the strength of interfacial film. The results show that the adsorption of functional silica nanoparticles at the oil–water interface clearly decreases the

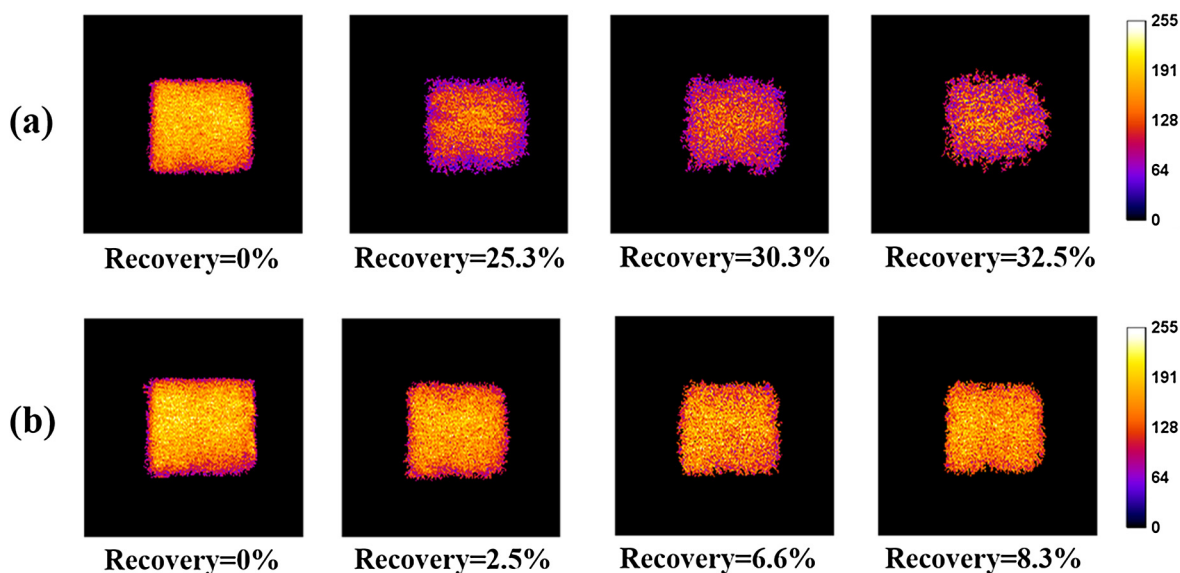


Fig. 9. 2D NMR pseudo color images of spontaneous imbibition at different imbibition stages (a) 0.1 wt% silica nanofluid, (b) 3 wt% NaCl solution.

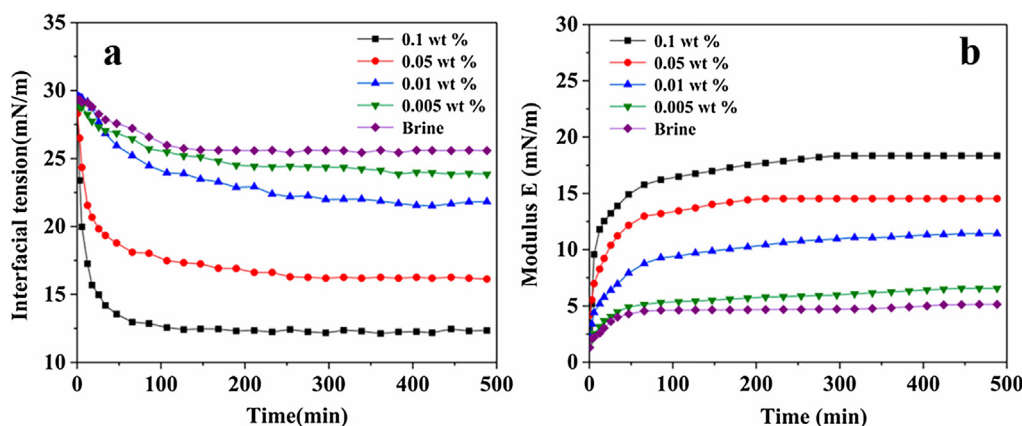


Fig. 10. Interfacial tension (a) and interfacial dilatational modulus (b) for interfaces between nanofluid or brine and kerosene at 60 °C. Frequency 0.1 Hz.

interfacial tension. Moreover, the adsorption of silica nanoparticles at the oil–water interface forms a strong interfacial film. This prevents the oil droplets from attaching to the rock surface and thus accelerating spontaneous imbibition. The functional silica nanoparticles showed an excellent interfacial activity, beneficial for EOR.

3.6.2. Wettability alteration

Fig. 11 shows the contact angle of oil droplets on oil-wet glass surface immersed in different fluids. To obtain an oil-wet surface, the glass slides were immersed in paraffin at 80 °C for 24 h. The oil droplet on solid surface was captured using an inverted needle. The contact angle of oil droplet on oil-wet glass surface treated with brine was $\sim 58^\circ$, indicating that the glass surface was still oleophilic. Fig. 11b shows the glass surface treated with 0.1 wt% silica nanofluid. A comparison shows that the adsorption of silica nanoparticles obviously altered the wettability of hydrophobic surface from oil-wet to water-wet.

Clearly, the wettability of rock can affect the NMR surface relaxation. The wettability state of a fluid-saturated rock can be obtained from the change in T_2 relaxation time (Zhang et al., 2000; Brown and Fatt, 1956). Fig. 12 shows the T_2 spectrum of kerosene in the cores and bulk kerosene (outside the core). The T_2 spectrum of bulk kerosene has a single peak between 623 ms and 1056 ms. Compared with bulk kerosene, the kerosene present in core shows a significant shift to shorter relaxation times. This phenomenon is caused by the surface relaxation of kerosene. The kerosene present in the pores of rock is bound to rock surface and moistens the surface. The wettability of rock changed from water-wet to oil-wet. Fig. 12a shows the oil distribution of core immersed in 0.1 wt% silica nanofluid during imbibition. Peak II has a significant reduction and shifts to longer relaxation times

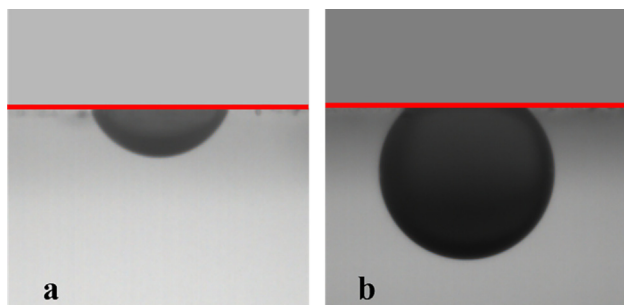


Fig. 11. Oil droplets on oil-wet glass surface treated with brine (a) and nanofluid (b).

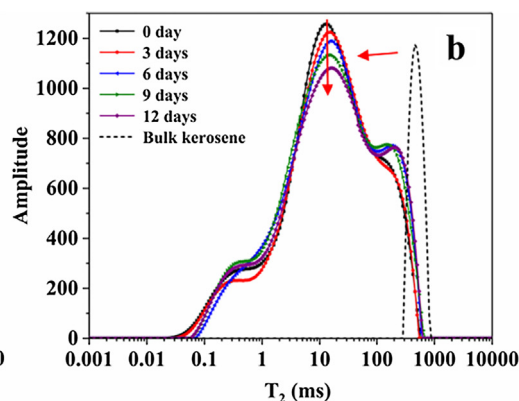
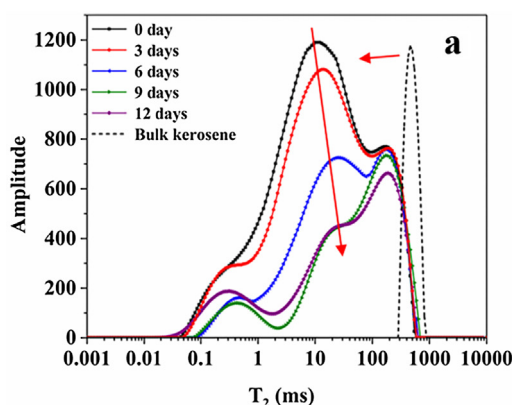


Fig. 12. T_2 spectrum before and after the imbibition of core immersed in 0.1 wt% silica nanofluid (a) and 3 wt% NaCl solution (b).

with the change in time. This phenomenon is not observed in the T_2 spectrum of core immersed in 3 wt% NaCl solution (Fig. 12b).

The shift of peak indicates a change in wettability. The relaxation time of peak II (Fig. 12a) approaches that of bulk kerosene, indicating that the oil droplets are stripped off from the rock surface and the surface relaxation effect is weakened. Nanofluid acts as the wetting fluid and is in contact with the rock surface of mesopores and changes the wettability of rock from oil-wet to water-wet. The relaxation time of peak II (Fig. 12b) slightly shifted at the first 6 days, but then did not shift. The brine does not completely contact the rock surface, but occupies the pores with oil together. The redistribution of oil and water resulted in the shift, but the wettability of rock did not change. The phenomenon observed by NMR is consistent with the results of wettability alteration experiment. The results indicate that the nanofluid based on functional silica nanoparticles could effectively change the oil-wet surface to a water-wet surface. A water-wet surface is conducive to improving capillary driving force and EOR (El-Hoshoudy et al., 2016; Hendraningrat and Torsæter, 2014).

3.6.3. Spreading of nanofluid at oil/nanofluid/solid three-phase contact region

The dynamic contact angle of oil droplet in different fluids (0.1 wt% silica nanofluid and brine) was measured to study oil displacement from a solid surface. Fig. 13 shows the effect of different fluids (0.1 wt% silica nanofluid and brine) for oil contact angle on oil-wet glass surface. When the oil droplet on glass surface was

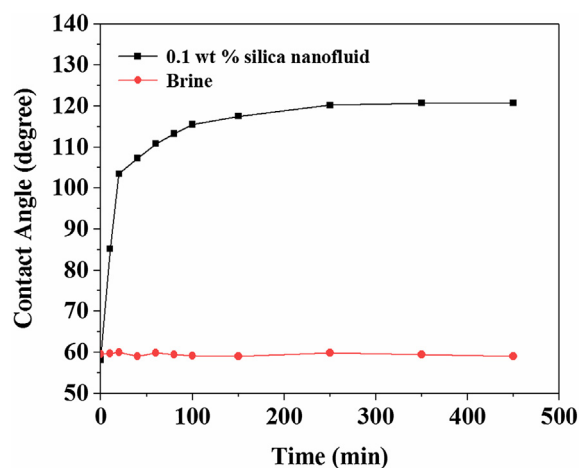


Fig. 13. Effect of different fluids (0.1 wt% silica nanofluid and brine) for oil contact angle on oil-wet glass surface.

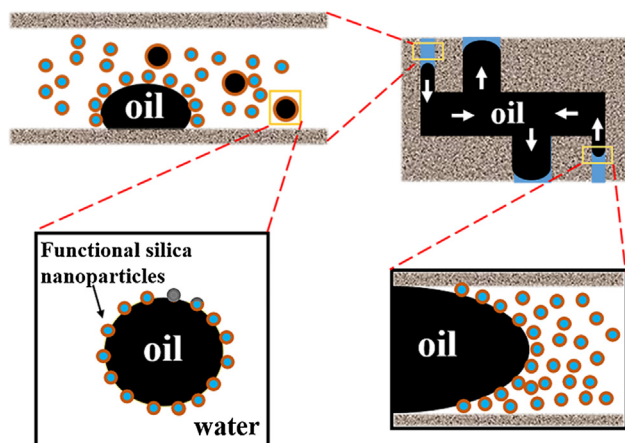


Fig. 14. Spontaneous imbibition mechanism of nanofluid.

immersed in 0.1 wt% silica nanofluid, the oil contact angle changed from 56° to 120° . In the initial stage at ~ 30 min, the contact angle of oil droplet on glass surface in the nanofluid increased rapidly, and it was observed that the oil droplet was displaced from the glass surface. Then, the contact angle increased slowly until it reached a plateau.

According to the experimental results, the spreading mechanism of nanofluid at oil/nanofluid/solid three-phase contact region is shown in Fig. 14. First, the adsorption of nanoparticles at the oil–water interface achieves a low interfacial tension and forms a strong interfacial film. The interfacial film also effectively prevents oil droplets from adhering to the rock surface again during the migration. Second, the adsorption of nanoparticles converts the wettability of rock surface from oil-wet to water-wet. The porous rock can be considered as a complex structure constructed with different sizes of capillaries in different directions. For a water-wet rock, the capillary force acts as the main driving force of displacement and becomes stronger and increases with the decrease in pore diameter. The water-based nanofluid was imbibed into ultralow permeable cores through small pores from all the directions. With the increase in the energy in pores, the oil in pores tended to flow out of the core through large pores. Third, the adsorption and accumulation of nanoparticles in oil/nanofluid/solid three-phase contact region formed a wedge film. The force that separates the oil droplets from solid surface is known as structural disjoining pressure as reported by Zhang et al. (2014), Wasan and Nikolov (2003), Chengara et al. (2004), Kondiparty et al. (2012), Liu et al. (2012), Kondiparty et al. (2011). The structural disjoining pressure is formed in the oil/nanofluid/solid three-phase contact region, pointing from nanofluid to oil under the combined action of Brownian motion and electrostatic repulsion among the nanoparticles. When interfacial activity, wettability alteration, capillary force, and structural separation pressure are available, the oil droplets can be effectively removed from the solid surface, and the recovery is significantly improved by nanofluid.

4. Conclusion

In this paper, NMR technique was used to monitor the migration trend of nanofluid in sandstone cores during spontaneous imbibition. The conclusions are as follows:

(1) Combined spontaneous imbibition experiments and NMR measurements effectively reflect the characteristics of oil distribution in oil/nanofluid/rock system. The pore system of sandstone can be divided into micropores, mesopores, and macropores, and 70.82–71.98 wt% of oil was distributed in mesopores ($50 \text{ nm} < \text{pore size} \leq 3000 \text{ nm}$);

(2) The final oil recoveries of core immersed in different concentrations of nanofluids and brine were 32.5%, 26.9%, 20.5%, 15.1%, and 8.3%. Combined with the results of T_2 spectrum, the recovery contributions of pores mainly focused on mesopores;

(3) The improved oil recovery mainly depends on the excellent properties of nanofluid based on functional silica nanoparticles, including interfacial activity, wetting alteration, and oil displacement efficiency.

The MRI results show that the oil was transported in the core pore with the help of nanofluid. Spontaneous imbibition experiments indicate that the oil recovery clearly improved using nanofluid as a chemical agent for EOR. With the development of oil and gas exploration, the proportion of ultralow permeability oil exploration and development will increase, especially in recent years the newly proved ultralow permeability oil reservoirs are particularly rich. The nanofluid based on functional silica nanoparticles, which has excellent properties, could improve the oil recovery of ultralow permeability oil reservoirs in the real oil industry. Hence, the functional silica nanoparticles provides a promising and efficient chemical agent for EOR of an ultralow permeable reservoir.

Supporting information

T_2 spectrum during the imbibition of core immersed in silica nanofluid with different concentrations and frequencies of oil distribution in pores before and after imbibition.

The interior wettability of kerosene-saturated cores (a) and after-imbibition cores (b) as the core is crushed.

Declaration of interest statement

We declare that we do not have any commercial or associative interest that represents a conflict of interest in connection with the work submitted.

Acknowledgment

This work was financially supported by the National Key Basic Research Program (No. 2015CB250904), National Science Fund (U1663206, 51425406), Chang Jiang Scholars Program (T2014152), and Climb Taishan Scholar Program in Shandong Province (tspd20161004).

Appendix A. Supplementary material

Supplementary data to this article can be found online at <https://doi.org/10.1016/j.ces.2019.02.036>.

References

- Al-Mahrooqi, S.H., Grattoni, C.A., Moss, A.K., Jing, X.D., 2003. An investigation of the effect of wettability on NMR characteristics of sandstone rock and fluid systems. *J. Petrol. Sci. Eng.* 39, 389–398.
- Bourbiaux, B.J., Kalaydjian, F.J., 1990. Experimental study of cocurrent and countercurrent flows in natural porous media. *SPE Reservoir Eng.* 5, 361–368.
- Brown, R.J.S., Fatt, I., 1956. Measurements of fractional wettability of oil fields' rocks by the nuclear magnetic relaxation method. Fall Meeting of the Petroleum Branch of AIME. Society of Petroleum Engineers.
- Cai, J., Yu, B., Zou, M., Mei, M., 2010. Fractal analysis of invasion depth of extraneous fluids in porous media. *Chem. Eng. Sci.* 65, 5178–5186.
- Chengara, A., Nikolov, A.D., Wasan, D.T., Trokhymchuk, A., Henderson, D., 2004. Spreading of nanofluids driven by the structural disjoining pressure gradient. *J. Colloid Interface Sci.* 280, 192–201.
- Dillinger, A., Esteban, L., 2014. Experimental evaluation of reservoir quality in Mesozoic formations of the Perth Basin (Western Australia) by using a laboratory low field Nuclear Magnetic Resonance. *Mar. Pet. Geol.* 57, 455–469.
- Ehtesabi, H., Ahadian, M.M., Taghikhani, V., Ghazanfari, M.H., 2014. Enhanced heavy oil recovery in sandstone cores using TiO_2 nanofluids. *Energy Fuels* 28, 423–430.

- El-Hoshoudy, A.N., Desouky, S.E.M., Betiha, M.A., Alsabagh, A.M., 2016. Use of 1-vinyl imidazole based surfmers for preparation of polyacrylamide-SiO₂ nanocomposite through aza-Michael addition copolymerization reaction for rock wettability alteration. *Fuel* 170, 161–175.
- Esfandiyari Bayat, A., Junin, R., Samsuri, A., Piroozian, A., Hokmabadi, M., 2014. Impact of metal oxide nanoparticles on enhanced oil recovery from limestone media at several temperatures. *Energy Fuels* 28, 6255–6266.
- Franco, C.A., Nassar, N.N., Ruiz, M.A., Pereiraalmaa, P., Cortés, F.B., 2013. Nanoparticles for inhibition of asphaltene damage: adsorption study and displacement test on porous media. *Energy Fuels* 27, 2899–2907.
- Giri, A., Tarafdar, S., Gouze, P., Dutta, T., 2012. Fractal pore structure of sedimentary rocks: simulation in 2-d using a relaxed bidisperse ballistic deposition model. *J. Appl. Geophys.* 87, 40–45.
- Guo, F., Aryana, S., 2016. An experimental investigation of nanoparticle-stabilized CO₂ foam used in enhanced oil recovery. *Fuel* 186, 430–442.
- Hammond, P.S., Unsal, E., 2009. Spontaneous and forced imbibition of aqueous wettability altering surfactant solution into an initially oil-wet capillary. *Langmuir* 25, 12591–12603.
- Hammond, P.S., Unsal, E., 2010. Forced and spontaneous imbibition of surfactant solution into an oil-wet capillary: the effects of surfactant diffusion ahead of the advancing meniscus. *Langmuir* 26, 6206–6221.
- Hammond, P.S., Unsal, E., 2011. Spontaneous imbibition of surfactant solution into an oil-wet capillary: wettability restoration by surfactant–contaminant complexation. *Langmuir* 27, 4412–4429.
- Hashemi, R., Nassar, N.N., Almaa, P.P., 2014. Nanoparticle technology for heavy oil in-situ upgrading and recovery enhancement: opportunities and challenges. *Appl. Energy* 133, 374–387.
- Hendraningrat, L., Torsæter, O., 2014. Effects of the initial rock wettability on silica-based nanofluid-enhanced oil recovery processes at reservoir temperatures. *Energy Fuels* 28, 6228–6241.
- Hendraningrat, L., Torsæter, O., 2013. Effect of some parameters influencing enhanced oil recovery process using silica nanoparticles: an experimental investigation. *SPE Reservoir Characterisation and Simulation Conference and Exhibition*.
- Hun, L., Shicheng, Z., Fei, W., Ziqing, P., Jianye, M., Tong, Z., Zongxiao, R., 2016. Experimental investigation on imbibition-front progression in shale based on nuclear magnetic resonance. *Energy Fuels* 30, 9097–9105.
- Karimi, A., Fakhroueian, Z., Bahramian, A., Pour Khiabani, N., Darabad, J.B., Azin, R., Arya, S., 2012. Wettability alteration in carbonates using zirconium oxide nanofluids: EOR implications. *Energy Fuels* 26, 1028–1036.
- Kondiparty, K., Nikolov, A., Wu, S., Wasan, D., 2011. Wetting and spreading of nanofluids on solid surfaces driven by the structural disjoining pressure: statics analysis and experiments. *Langmuir* 27, 3324–3335.
- Kondiparty, K., Nikolov, A.D., Wasan, D., Liu, K.L., 2012. Dynamic spreading of nanofluids on solids. Part I: experimental. *Langmuir* 28, 14618–14623.
- Lai, F., Li, Z., Wei, Q., Zhang, T., Zhao, Q., 2016. Experimental investigation of spontaneous imbibition in tight reservoir with nuclear magnetic resonance testing. *Energy Fuels*.
- Lai, J., Wang, G., Fan, Z., Chen, J., Wang, S., Zhou, Z., Fan, X., 2016. Insight into the pore structure of tight sandstones using NMR and HPMT measurements. *Energy Fuels* 30.
- Lai, J., Wang, G., Cao, J., Xiao, C., Wang, S., Pang, X., Dai, Q., He, Z., Fan, X., Yang, L., 2018. Investigation of pore structure and petrophysical property in tight sandstones. *Mar. Pet. Geol.* 91, 179–189.
- Li, K., 2010. Analytical derivation of Brooks-Corey type capillary pressure models using fractal geometry and evaluation of rock heterogeneity. *J. Petrol. Sci. Eng.* 73, 20–26.
- Li, Y., Dai, C., Zhou, H., Wang, X., Lv, W., Zhao, M., 2017. Investigation of spontaneous imbibition by using a surfactant-free active silica water-based nanofluid for enhanced oil recovery. *Energy Fuels*.
- Li, K., Horne, R.N., 2006. Fractal modeling of capillary pressure curves for The Geysers rocks. *Geothermics* 35, 198–207.
- Liang, B., Jiang, H., Li, J., Gong, C., Jiang, R., Qu, S., Pei, Y., Yang, H., 2017. Investigation of oil saturation development behind spontaneous imbibition front using nuclear magnetic resonance (NMR) T2.
- Liu, K.L., Kondiparty, K., Nikolov, A.D., Wasan, D., 2012. Dynamic spreading of nanofluids on solids part ii: modeling. *Langmuir* 28, 16274.
- Maas, M., Ooi, C.C., Fuller, G.G., 2010. Thin film formation of silica nanoparticle/lipid composite films at the fluid-fluid interface. *Langmuir* 26, 17867–17873.
- Meng, M., Ge, H., Ji, W., Wang, X., 2016. Research on the auto-removal mechanism of shale aqueous phase trapping using low field nuclear magnetic resonance technique. *J. Petrol. Sci. Eng.* 137, 63–73.
- Monfared, A.D., Ghazanfari, M.H., Jamialahmadi, M., Helalizadeh, A., 2016. The potential application of silica nanoparticles for wettability alteration of oil-wet calcite: a mechanistic study. *Energy Fuels* 30.
- Nakata, K., Fujishima, A., 2012. TiO₂ photocatalysis: design and applications. *J. Photochem. Photobiol., C* 13, 169–189.
- Perino, A., Noik, C., Dalmazzone, C., 2013. Effect of fumed silica particles on water-in-crude oil emulsion: emulsion stability, interfacial properties, and contribution of crude oil fractions. *Energy Fuels* 27, 2399–2412.
- Rahmatmand, B., Keshavarz, P., Ayatollahi, S., 2016. Study of absorption enhancement of CO₂ by SiO₂, Al₂O₃, CNT, and Fe₃O₄ nanoparticles in water and amine solutions. *J. Chem. Eng. Data* 61, 1378–1387.
- Saidian, M., Prasad, M., 2015. Effect of mineralogy on nuclear magnetic resonance surface relaxivity: a case study of Middle Bakken and Three Forks formations. *Fuel* 161, 197–206.
- Sharma, T., Iglaer, S., Sangwai, J.S., 2016. Silica nanofluids in an oilfield polymer polyacrylamide: interfacial properties, wettability alteration and applications for chemical enhanced oil recovery. *Ind. Eng. Chem. Res.* 55.
- Suleimanov, B.A., Ismailov, F.S., Veliyev, E.F., 2011. Nanofluid for enhanced oil recovery. *J. Petrol. Sci. Eng.* 78, 431–437.
- Tinni, A., Odusina, E., Sulucarnain, I., Sondergeld, C., Rai, C.S., 2015. Nuclear-magnetic-resonance response of brine, oil, and methane in organic-rich shales. *SPE Reservoir Eval. Eng.* 18.
- Wang, Z., Pan, M., Shi, Y., Liu, L., Xiong, F., Qin, Z., 2018. Fractal analysis of donghetang sandstones using NMR measurements. *Energy Fuels*.
- Wang, X., Peng, X., Zhang, S., Du, Z., Zeng, F., 2018. Characteristics of oil distributions in forced and spontaneous imbibition of tight oil reservoir. *Fuel* 224, 280–288.
- Wasan, D.T., Nikolov, A.D., 2003. Spreading of nanofluids on solids. *Nature* 423, 156–159.
- Wei, B., Li, Q., Jin, F., Li, H., Wang, C., 2016. The potential of a novel nanofluid in enhancing oil recovery. *Energy Fuels* 30.
- Wong, K.V., Leon, O.D., 2010. Applications of nanofluids: current and future. *Adv. Mech. Eng.* 2010, 1652–1660.
- Yang, L., Ge, H., Shi, X., Cheng, Y., Zhang, K., Chen, H., Shen, Y., Zhang, J., Qu, X., 2016. The effect of microstructure and rock mineralogy on water imbibition characteristics in tight reservoirs. *J. Nat. Gas Sci. Eng.* 34, 1461–1471.
- Zargartalebi, M., Kharrat, R., Barati, N., 2015. Enhancement of surfactant flooding performance by the use of silica nanoparticles. *Fuel* 143, 21–27.
- Zhang, G.Q., Huang, C.C., Hirasaki, G.J., 2000. Interpretation of wettability in sandstones with NMR analysis. *Biochim. Et Biophysica Acta* 1445, 86–98.
- Zhang, H., Nikolov, A., Wasan, D., 2014. Enhanced oil recovery (EOR) using nanoparticle dispersions: underlying mechanism and imbibition experiments. *Energy Fuels* 28, 3002–3009.
- Zhang, Z., Weller, A., 2014. Fractal dimension of pore-space geometry of an Eocene sandstone formation. *Geophysics* 79, D377–D387.
- Zhao, P., Wang, Z., Sun, Z., Cai, J., Wang, L., 2017. Investigation on the pore structure and multifractal characteristics of tight oil reservoirs using NMR measurements: Permian Lucaogou Formation in Jimusar Sag, Junggar Basin. *Marine Petrol. Geol.* 86, 1067–1081.
- Zhou, L., Kang, Z., 2016. Fractal characterization of pores in shales using NMR: a case study from the Lower Cambrian Niutitang Formation in the Middle Yangtze Platform, Southwest China. *J. Nat. Gas Sci. Eng.* 35, 860–872.